International Journal of Biological Macromolecules 307 (2025) 142076

Contents lists available at ScienceDirect

International Journal of Biological Macromolecules

journal homepage: www.elsevier.com/locate/ijbiomac

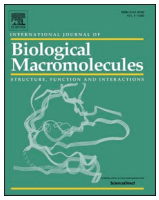

Rational design of DAHP synthase and prephenate dehydrogenase for metabolic engineering of *Bacillus amyloliquefaciens* to produce L-tyrosine☆

Anying Ji [1], Dian Zou [1], Aimin Ma, Xuetuan Wei [*]

National Key Laboratory of Agricultural Microbiology, Huazhong Agricultural University, Wuhan 430070, China

ARTICLE INFO

Keywords:
Enzyme evolution
Rational design
L-tyrosine
DAHP synthase
Prephenate dehydrogenase
Metabolic engineering

ABSTRACT

The rational design of enzymes represents a critical strategy for achieving efficient and sustainable biocatalysis. In this study, enzyme evolution guided by rational design was utilized to engineer two key enzymes, DAHP synthase (AroA) and prephenate dehydrogenase (TyrA), within the biosynthetic pathway of L-tyrosine. The beneficial mutants $AroA^{R27A/K38A}$ and $TyrA^{I309A/E330V}$ were identified, leading to a 102 % and 105 % increase in L-tyrosine yield, respectively. Molecular dynamics simulations further explained the possible mechanism underlying their improved catalytic efficiency. Co-expression of these two mutant genes resulted in a significant increase in L-tyrosine yield. Additionally, modifications in the branching metabolic pathways, which altered both material and energy flux, further enhanced L-tyrosine production. Ultimately, the L-tyrosine yield (0.14 g/g) from xylose was much higher than that from glucose, and the final L-tyrosine titer (9.39 g/L) and productivity (0.26 g/(L·h)) were achieved through fermentation optimization in shake flasks. This represents the highest reported yield in shake flasks. The strategies described here will contribute to the development of microbial strains for the efficient production of L-tyrosine from sustainable biomass resources.

1. Introduction

L-tyrosine is an indispensable amino acid for human nutrition [1–3]. It has widespread applications in various fields, including foods, feeds, chemicals, cosmetics, and pharmaceuticals [4–6]. Moreover, it serves as a crucial platform chemical for the production of diverse functional chemicals such as resveratrol, caffeic acid, and flavonoids [7–11]. The global L-tyrosine market is projected to reach $16 million by 2030, with a compound annual growth rate (CAGR) of 6.4 %. Additionally, the price of L-tyrosine in China is approximately ¥60,000 per ton. In recent years, the demand for L-tyrosine has gradually increased [3,12,13]. Traditionally, chemical synthesis has been associated with serious issues of high pollution and low safety, including the use of catalysts such as sulfuric acid and nitric acid, as well as the generation of harmful substances such as ammonia and cyanide [3,14,15]. Therefore, it is essential to develop green and sustainable approaches for L-tyrosine synthesis in order to reduce environmental pollution and enhance the utilization of renewable feedstocks [3,16].

Microbial fermentation has emerged as a highly promising strategy [3,16,17], and it offers several advantages, such as the use of sustainable biomass substrates and environmentally friendly fermentation process [3,15,18]. However, present fermentation yields of L-tyrosine are relatively low, which hinders the commercial production of L-tyrosine through microbial fermentation. Therefore, it is urgent to develop novel and efficient microbial cell factories for the biosynthesis of L-tyrosine [15,19,20]. Currently, *Escherichia coli* is the primary chassis for the biosynthesis of L-tyrosine [3,21,22]. However, the existence of endotoxins usually requires a complex separation process, which increases its production cost in foods and feeds applications [1,23,24]. In addition, recent studies have made significant progress in elucidating the biosynthesis of L-tyrosine in *Corynebacterium glutamicum*. By upregulating the expression of key genes in the L-tyrosine biosynthesis pathway and utilizing a mixed carbon source of xylose and glucose, researchers have successfully redirected carbon flux toward the L-tyrosine synthesis pathway, thereby significantly enhancing L-tyrosine production. However, there is a problem of excessively low production yield, with the current highest yield being only 3.6 g/L [2]. *Bacillus* species such as *B. subtilis and B. amyloliquefaciens* have emerged as promising microbial

☆ This article is part of a special issue entitled: EnzEvo: Sustainable Biocatalysis published in International Journal of Biological Macromolecules.

* Corresponding author at: No. 1 Shizishan Street, Hongshan District, Wuhan 430070, Hubei, China.
E-mail address: weixuetuan@mail.hzau.edu.cn (X. Wei).

[1] These authors contribute equally to this work.

https://doi.org/10.1016/j.ijbiomac.2025.142076
Received 12 December 2024; Received in revised form 2 March 2025; Accepted 11 March 2025
Available online 14 March 2025

cell factories due to their GRAS status (Generally Recognized as Safe), rapid growth, high secretion ability, and strong robustness [18,24,25]. One previous study has demonstrated that *B. amyloliquefaciens* HZ-12 can serve as a novel chassis for L-tyrosine synthesis [1], although the fermentation titer requires further improved.

In *Bacillus* species, L-tyrosine is predominantly synthesized through a complex aromatic compound pathway involving thirteen sequential reactions and intricate metabolic regulation [8,26–28]. Therein, the 3-deoxy-D-arabinoheptulosonate-7-phosphate (DAHP) synthase (AroA) and the prephenate dehydrogenase (TyrA) serve as the rate-limiting enzymes, similar to *E. coli* [29,30]. AroA has been extensively investigated in *E. coli*, and it has three isoenzymes, namely AroG, AroF, and AroH [31,32]. These isoenzymes are subject to feedback inhibition by *L*-phenylalanine, L-tyrosine, and L-tryptophan [33]. Meanwhile, the TyrA is a bifunctional enzyme with activities of prephenate dehydrogenase and chorismate mutase, which is also inhibited by feedback from L-tyrosine [34]. In *E. coli*, the primary strategy for L-tyrosine production is to relieve the feedback inhibition [30]. However, the TyrA and AroG mutants commonly used in *E. coli* are mainly obtained by error-prone PCR, which yiled only limited mutation sites. We also attempted to enhance L-tyrosine accumulation in *B. amyloliquefaciens* by expression of TyrA and AroG mutants from *E. coli*, resulting in a production yield of 475 mg/L [1]. Therefore, there is still a gap in understanding the complex regulatory mechanisms of DAHP synthase and prephenate dehydrogenase, and identifying beneficial mutants of AroA and TyrA has become a limiting factor in the synthesis of L-tyrosine.

At present, enzyme evolution is the primary means to improve the catalytic efficiency of enzymes [3]. Rational design based on protein structure can generate “ small and acute ” mutant libraries, which overcomes the limitations posed by the low transformation efficiency of *Bacillus* spp.. Through homology modeling, molecular docking, and alanine scanning mutations, three critical residues (E69, K73, and L171) were identified in UDP-glycosyltransferase (UGT109A1) from *B. subtilis*, and the beneficial mutant UGT109A1-K73A significantly enhanced the biosynthesis of protopanaxadiol [35]. In addition, a smart library was constructed by semi-rational design to improve the catalytic activity of type II L-asparaginase from *Bacillus licheniformis,* and successfully obtained a quintuple mutant with a 4.24-fold increase in enzyme activity [36]. These findings demonstrate the rational design is a promising method for molecular modification of key enzymes in *Bacillus* spp.. In this study, enzyme evolution based on rational design was employed to modify AroA and TyrA in *B. amyloliquefaciens*, and beneficial mutants were obtained to promote the L-tyrosine synthesis. In combination with the pathway engineering strategies, yielding the optimal engineering strain. The final L-tyrosine production was subsequently investigated by using xylose as a carbon source combined with fermentation optimization. This study not only provides two efficient enzyme mutants, but also establishes a sustainable, green, and efficient approach for the biosynthesis of L-tyrosine.

2. Materials and methods

2.1. Chemicals

In this work, the TransStartFastPfu DNA polymerase and TransStartR easyTaq DNA polymerase were procured from TransGen Biotech Co., Ltd. (Beijing, China). The DNA restriction enzymes, T4 ligase, dNTPs, RNase, and DL5000 Marker were provided by Takara Biotechnology Co., Ltd. (Dalian, China). The DNA recovery kit and plasmid extraction kit were purchased from Omega Bio-Tek in Guangzhou, China. Other chemicals were obtained from Sinopharm Chemical Reagent Co., Ltd. (Shanghai, China).

2.2. Strains and plasmids

The strains, plasmids, and primers used in this study are listed in Tables S1, S2, and S3 of the Supplementary Materials. All the gene deletion mutants and overexpression strains were derived from the wild-type strain *B. amyloliquefaciens* HZ-12. The vectors based on pHY300PLK and T2(2) were constructed using *E. coli* DH5α as the cloning host strain.

2.3. Construction of recombinant expression strains

The construction process of plasmids pHY300PLK and T2(2) followed previously established methods [37]. AroA and TyrA mutants were generated via overlap-extension PCR. In this study, the construction of AroA mutants is described as a representative example, with TyrA mutants generated analogously. The plasmid pHY-P43-*Bao-aroA*-T*amyL* was used as a template, and the primers P43-*Bao-aroA*(R27A)-F, *Bao-aroA*(R27A)-MR1, *Bao-aroA*(R27A)-MF1, and TL-*Bao-aroA*(R27A)-R were used for the first-round of PCR reaction. The two PCR products were purified using a DNA purification kit. Then, these two fragments were used as templates for a second-round overlap-extension PCR reaction with primers P43-*Bao-aroA*(R27A)-F and TL-*Bao-aroA*(R27A)-R. The expression plasmid pHY-P43-*Bao-aroA*^{R27A} was obtained by further ligation of the digested *aroA* mutant fragment with the pHY300PLK plasmid at the restriction sites *Bam*HI and *Xba*I. Finally, the plasmid was electrically transformed into competent cells of *B. amyloliquefaciens* HZ-12 to generate the mutant strain HZ/pHY-P43-*Bao-aroA*^{R27A}. All other mutants were constructed following the same protocol.

The construction of the T2(2) vector is exemplified by the deletion of the *pheA* gene. Using the HZ-12 genome as a template, the upstream and downstream homologous arms were amplified with primer pairs *pheA*-AF/*pheA*-AR and *pheA*-BF/*pheA*-BR, respectively. The amplified products were then fused and ligated using SOE-PCR. Subsequently, the fused product was transformed into the T2(2) plasmid via double digestion and ligation. After sequencing verification, the correctly constructed plasmid T2(2)-ori*ΔpheA* was obtained. Finally, this plasmid was electroporated into competent cells of HZ-12, and single- and double-crossover events were carried out through homologous recombination to obtain the engineered strain HZ*ΔpheA*. On this basis, the plasmid S6–36 was electroporated into HZ*ΔpheA* to obtain the engineered strain HZ*ΔpheA*/S6–36.

2.4. Homologous modeling and molecular docking

The amino acid sequences of AroA and TyrA was submitted into SWISS-MODEL (https://swissmodel.expasy.org/) for homology-based 3D structure prediction. The optimal model was selected based on highest sequence identity, Global Model Quality Estimation (GMQE) score, and Qualitative Model Energy Analysis (QMEAN) score were selected as the best-fitting model [38]. Model validation was performed using the SAVES v6.0 server (https://saves.mbi.ucla.edu/) from the UCLA-DOE LAB Structure Analysis and Verification Suite. The 3D structure of the substrate molecule prephenate was obtained from the PubChem database.

Hydrogen atoms were added to the AroA and TyrA protein models using AutoDockTools, with both polar and non-polar hydrogens retained. The models were saved as receptors in PDBQT format. The prephenate molecule was also added with all hydrogens and gasteiger charges using the Autodock tools and saved as ligands in PDBQT format. Charge assignment and residue parameterization for receptors and ligands were automated within the AutoDock framework. A grid box used for molecular docking was adjusted to contain the active pocket of the homologous protein. The Genetic Algorithm module in the Autodock 4.2.6 software was used to perform the docking of AroA, TyrA, and its ligand prephenate. The conformations with the highest scores and the lowest binding energies were selected as the most reliable conformation for complexes. Meanwhile, the generated docking results were uploaded to the Protein-Ligand Interaction Profiler (PLIP) (https://plip-tool.biotec.tu-dresden.de/plip-web/plip/index) for detailed analysis of interaction forces and recognition sites. The visualization modules of

PyMol and Discovery Studio 2018 (BIOVIA Corp., San Diego, CA, USA) were used to analyze the interactions and key amino acid sites in detail.

2.5. Molecular dynamics simulation

The initial structure for the all-atom molecular dynamics simulations was derived from docking results, representing the protein-ligand complex. The simulations were carried out using AMBER 18 software. Prior to simulation, the AM1-BCC charge of the small molecule was computed using the antechamber module. The small molecule and protein were then described using the GAFF2 force field for the small molecule and the ff14SB force field for the protein. Hydrogen atoms were added to the system using the LEaP module, and a truncated octahedral TIP3P solvent box was placed around the system with a 10 Å distance. Na^+/Cl^- ions were added to neutralize the system's charge, and topology and parameter files for simulation were generated. Prior to simulation, the energy of the system was optimized through a combination of 2500 steps of steepest descent and conjugate gradient methods. The system was then heated for 200 ps at fixed volume and constant heating rate, gradually increasing the temperature from 0 K to 298.15 K. The NVT (Isothermal-Isochoric) lineage simulation was performed with a duration of 500 ps at a temperature of 298.15 K. Uniform distribution of solvent molecules in the solvent box. Finally, the NPT (Isothermal-Isobaric) equilibrium simulation was performed on the entire system for an additional 500 ps before performing the NPT descent simulations of two separate composite systems, lasting a total of 100 ns under periodic boundary conditions. During these simulations, the nonbonding truncation distance was set at 10 Å, and the long-range electrostatic interaction was calculated by the Particle Mesh Ewald (PME) method. Then, the hydrogen bond length was limited by SHAKE method, and the collision frequency γ was set to 2 ps^{-1} by the Langevin algorithm, which regulated the temperature. The system pressure remained constant at 1 atm while integral step size remained 2 fs, and tracks were saved every10 ps for subsequent analysis.

2.6. L-tyrosine fermentation

The strains were stored in an ultra-low temperature freezer at −80 °C. For fermentation, glycerol stocks were streaked on LB solid plates (10 g/L NaCl, 10 g/L peptone, 5 g/L yeast extract, and 15 g/L agar) to obtain isolated colonies. Subsequently, a single colony was inoculated into 50 mL of LB liquid medium containing 10 g/L tryptone, 5 g/L yeast extract, and 10 g/L NaCl. The inoculum cultures were obtained after 12 h of cultivation at 37 °C and 180 rpm. Then, 3 % (*v*/v) inoculums were inoculated into the 50 mL L-tyrosine fermentation medium containing 22 g/L glucose, 3 g/L $(NH_4)_2SO_4$, 6.75 g/L K_2HPO_4, 1.25 g/L KH_2PO_4, 1.5 g/L $MgSO_4{\cdot}7H_2O$, 5 g/L sodium citrate, 3 g/L peptone, 6 g/L yeast extract, 4 g/L $FeSO_4{\cdot}7H_2O$, 4 g/L $CaCl_2$, 1 g/L $MnSO_4{\cdot}5H_2O$, 0.4 g/L $CoCl_2{\cdot}6H_2O$, 0.2 g/L $ZnSO_4{\cdot}7H_2O$, 0.1 g/L $AlCl_3{\cdot}6H_2O$, 0.1 g/L $CuCl_2{\cdot}H_2O$, and 0.05 g/L H_3BO_4. Fermentation conditions were controlled at 37 °C and 180 rpm for 36 h, and the tetracycline was added at the final concentrations of 20 μg/mL.

2.7. Determination of L-tyrosine

The L-tyrosine concentration was quantified using High-performance liquid chromatography (HPLC) method. Firstly, 1 mL of fermentation broth was vigorously mixed with 0.6 mL of 1 M HCl for 1 h, followed by centrifugation at 10,000 *g* for 3 min. The resulting supernatant was then filtered through a 0.22 μm membrane. The HPLC analysis was performed using an Agilent 1100 HPLC chromatograph equipped with a ZORBAX Eclipse XDB-C18 (4.6 mm × 250 mm, 5 μm) column, and a UV detector wavelength was set at 280 nm. The mobile phase consisted of methanol (10 %) and sodium acetate (100 mM, pH 4.0). A flow rate of 0.6 mL/min and an injection volume of 10 μL were used, while the column temperature was maintained at 30 °C. The L-tyrosine concentration in the samples was calculated by a standard curve prepared with pure L-tyrosine.

2.8. Statistical analysis procedures

Each experiment was performed at least three independent biological replicates. Statistical analysis, including calculation of mean values, standard deviations, and assessment of statistical significance, were performed using SPSS 20.0 (IBM, Armonk, NY, USA). Data visualization and graphical representations were generated using GraphPad Prism 8.0 (GraphPad Software, USA).

3. Results and discussion

3.1. Reducing the inhibitory effect of prephenate on AroA to enhance the L-tyrosine synthesis by rational design

3.1.1. Identification of the key crucial sites of AroA by alanine scanning

Multifunctional proteins play diverse roles in metabolism [39]. According to the KEGG database, DAHP synthase (AroA) in *B. amyloliquefaciens* exhibits catalytic activities of both DAHP synthase and chorismate mutase. Specifically, DAHP synthase initiates the aromatic metabolite biosynthetic pathway by catalyzing the condensation of phosphoenolpyruvate (PEP) and erythrose 4-phosphate (E4P) to form 3-deoxy-D-arabino-heptulosonate-7-phosphate [27,40,41]. In contrast, chorismate mutase functions within a specialized branch of the pathway to synthesize the amino acids L-tyrosine and *L*-phenylalanine. Prephenate, the product of this reaction, acts as an allosteric inhibitor for DAHP when it binds to the active site on full-length protein [42]. This binding induces conformational changes, strengthening interactions between dimeric CM domains and tetrameric DAHP, which occludes the active site and disrupts DAHP function [39,43]. Therefore, reduction of the binding affinity between DAHP synthase and prephenate may weaken its inhibitory effect on DAHP synthase activity. Rational design has proven effective for enhancing enzyme performance [19,44,45]. Therefore, rational design was carried out on AroA to improve its catalytic efficiency through structural directing.

Due to the complexity of metabolic pathways, intracellular enzyme activity may not always correlate positively with the biosynthesis titer of the target metabolite [3]. Therefore, beneficial mutants of AroA were directly screened in *B. amyloliquefaciens* HZ-12 using the L-tyrosine titer as an indicator. First, the amino acid sequence of AroA was submitted to the SWISS-MODEL online server for homology modeling [38]. Subsequently, molecular docking was conducted using Autodock Vina 1.2.2 to dock prephenate with AroA [46]. The interaction between prephenate and AroA involves hydrophobic interactions by residues Arg 10, Arg 27, Lys38, Arg50 and hydrogen bonds by residues Arg 10, Arg 27, Lys38, Arg50 and Gln86 (Fig. 1A). Alanine is commonly used to investigate the effects of side chains on protein function due to its small side chain size. To identify the key amino acid residues of AroA, Ala scanning was employed to construct a refined library by selecting residues within 5 Å of the substrate. These mutants were expressed in *B. amyloliquefaciens* HZ-12, and the L-tyrosine levels were measured. As shown in Fig. 1B, most mutants did not exhibit an increase in L-tyrosine production, while the recombinant strains HZ/pHY-P43-*Bao-aroA*^{R27A} and HZ/pHY-P43-*Bao-aroA*^{K38A} demonstrated significantly higher titers of L-tyrosine compared to the control strain (HZ/pHY-P43-*Bao-aroA*), reaching 527 mg/L and 509 mg/L, respectively. These findings suggest that Arg27 and Lys38 may serve as crucial amino acid residues modulating AroA enzymatic activity, which could subsequently enhance L-tyrosine biosynthesis efficiency. Therefore, Arg27 and Lys38 were selected as targets for further study.

To further explain the validity of the sites Arg27 and Lys38, additional docking simulations of the mutant proteins with their substrate were conducted to analyze interaction forces, with a parallel comparison to the wild-type AroA/prephenate complex. As shown in Fig. 1C,

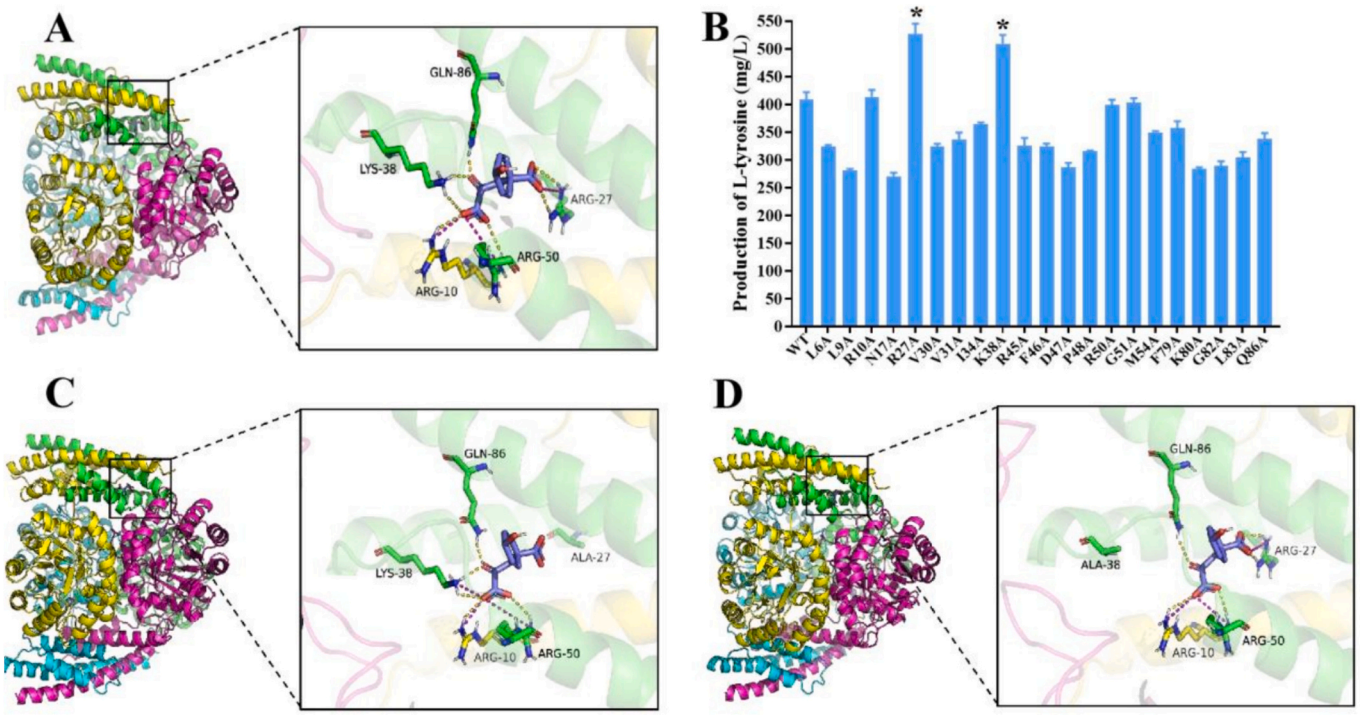

Fig. 1. Structural prediction and key residue sites determination of AroA. A: The overall structure of AroA/prephenate complex. B: Effects of AroA mutations on L-tyrosine synthesis. C: The overall structure of AroA^{R27A}/prephenate complex. D: The overall structure of AroA^{K38A}/prephenate complex. (The yellow dotted line represents hydrogen bond interactions, whereas the magenta dotted line indicates salt bridge interactions. *($p < 0.05$) indicates the significant levels compared with the control.)

prephenate formed hydrogen bonds with Lys38, Arg50, Gln86, and Arg10 in the AroA^{R27A} mutant, along with salt bridges mediated by Lys38, Arg50, and Arg10. In contrast, the AroA^{K38A} mutant exhibited hydrogen bonds with Arg27, Arg50, Gln86, and Arg10, and salt bridges with Arg27, Arg50, and Arg10 (Fig. 1D). These interactions facilitated tighter enzyme-substrate binding. Apparently, the R27A mutation resulted in the loss of the Arg27-mediated hydrogen bond and a salt bridge between prephenate and the binding pocket, while the K38A mutation similarly abolished the Lys38-dependent hydrogen bond and a salt bridge. We speculate that this may weaken the binding efficacy of prephenate, thereby altering molecular interactions at the biological level.

Notably, the loss of hydrogen bonds and salt bridges between Arg27, Lys38, and prephenate may not have affected the interaction between the AroA and its substrate (PEP and E4P). The binding sites for the substrate and prephenate exhibit significant differences in both

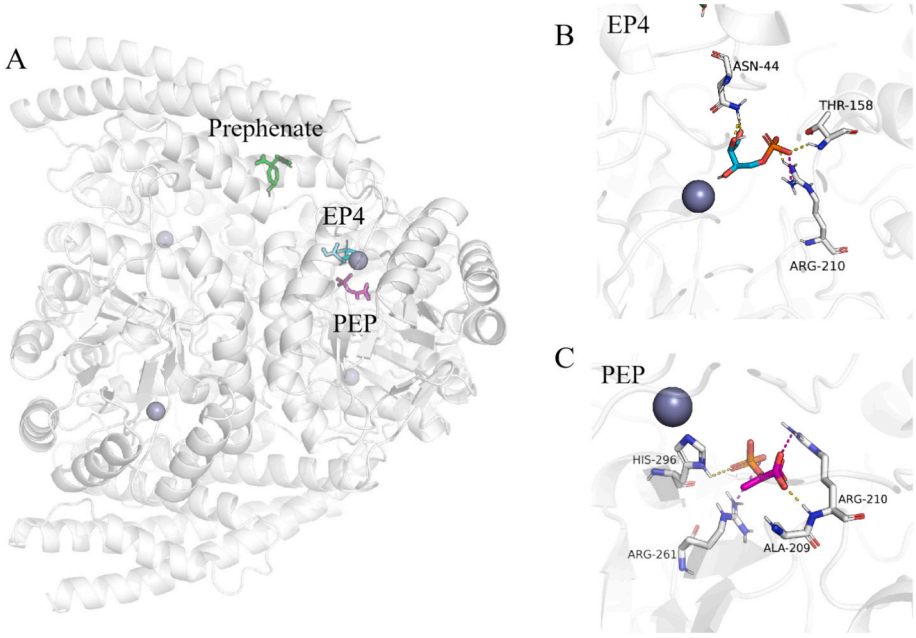

Fig. 2. Interaction diagram of substrate and AroA. (A) Binding positions of prephenate, EP4, and PEP on the protein surface. (B) Interaction diagram of E4P with AroA. (C) Interaction diagram of PEP with AroA. The dashed yellow lines represent hydrogen bonds, while the magenta lines indicate salt bridges.

structure and position, indicating that the possible competitive interaction may be reduced (Fig. 2A). It can be seen from Fig. 2B and C that the two substrates bind to the same site, and the binding site is partially duplicated. These findings demonstrate that the substrate complex may be independent of the inhibitor. Therefore, the absence of conserved hydrogen bonds and salt bridges involving Arg27 and Lys38 may enhance the flexibility of enzyme active sites, thereby improving the catalytic efficiency [47]. These findings explain the possible molecular mechanisms underlying residue effectiveness and provide a theoretical foundation for engineering AroA to improve catalytic performance.

3.1.2. Combined mutation of Arg27 with Lys38 and mechanism analysis

Based on the above analysis, we observed that modifications to side chain residues enhanced L-tyrosine synthesis. Wang et al. employed a similar strategy to validate the superior performance of the RoHpaB^{Y215A} mutant [48]. To further improve the L-tyrosine production, we introduced mutations at residues R27A and K38A to reduce in the side chain length by substituting phenylalanine, leucine, valine, and glycine. Subsequently, these mutant expression plasmids were electrically transformed into *B. amyloliquefaciens* HZ-12, generating a series of recombinant strains. The L-tyrosine production was measured in all strains after 36 h of shake-flask cultivation under identical conditions. The results revealed that substitution of R27 and K38 to phenylalanine, leucine, valine, or glycine did not significantly increase yield compared to alanine substitution (Fig. 3A), confirming the effectiveness of alanine replacement. Subsequently, additional combined mutations were performed to obtain corresponding recombinant expression strains HZ/pHY-P43-*Bao-aroA*$^{R27A/K38A}$. As shown in Fig. 3B, the engineering strain exhibited a 45 % increase in L-tyrosine titer (587 mg/L) compared to the control strain HZ/pHY-P43-*Bao-aroA,* indicating a synergistic enhancement. Furthermore, these mutants exhibited better effects compared to mutants derived from *E. coli*. In summary, we obtained the beneficial mutant AroA$^{R27A/K38A}$, which significantly improves L-tyrosine biosynthesis.

To gain deeper mechanistic insights, we performed molecular dynamics simulations to analyze the behavior of AroA$^{R27A/K38A}$. The root mean square deviation (RMSD) can serve as an indicator for the motion process of simulated objects. Higher RMSD values indicate greater conformational flexibility, while lower RMSD values suggest a more stable motion [49]. The time-dependent changes in RMSD for the AroA$^{R27A/K38A}$/prephenate and AroA^{WT}/prephenate complex systems during 100 ns molecular dynamics simulations are shown in Fig. 3C. Both systems gradually converged over the course of 100 ns and maintain stable fluctuations around 3 Å. Notably, the AroA$^{R27A/K38A}$/prephenate system exhibited smaller fluctuation difference compared to AroA^{WT}/prephenate, indicating that AroA^{WT}/prephenate complex is more susceptible to allosteric effects. Prephenate may make the conformational transformation of AroA^{WT} more significant to inhibit the

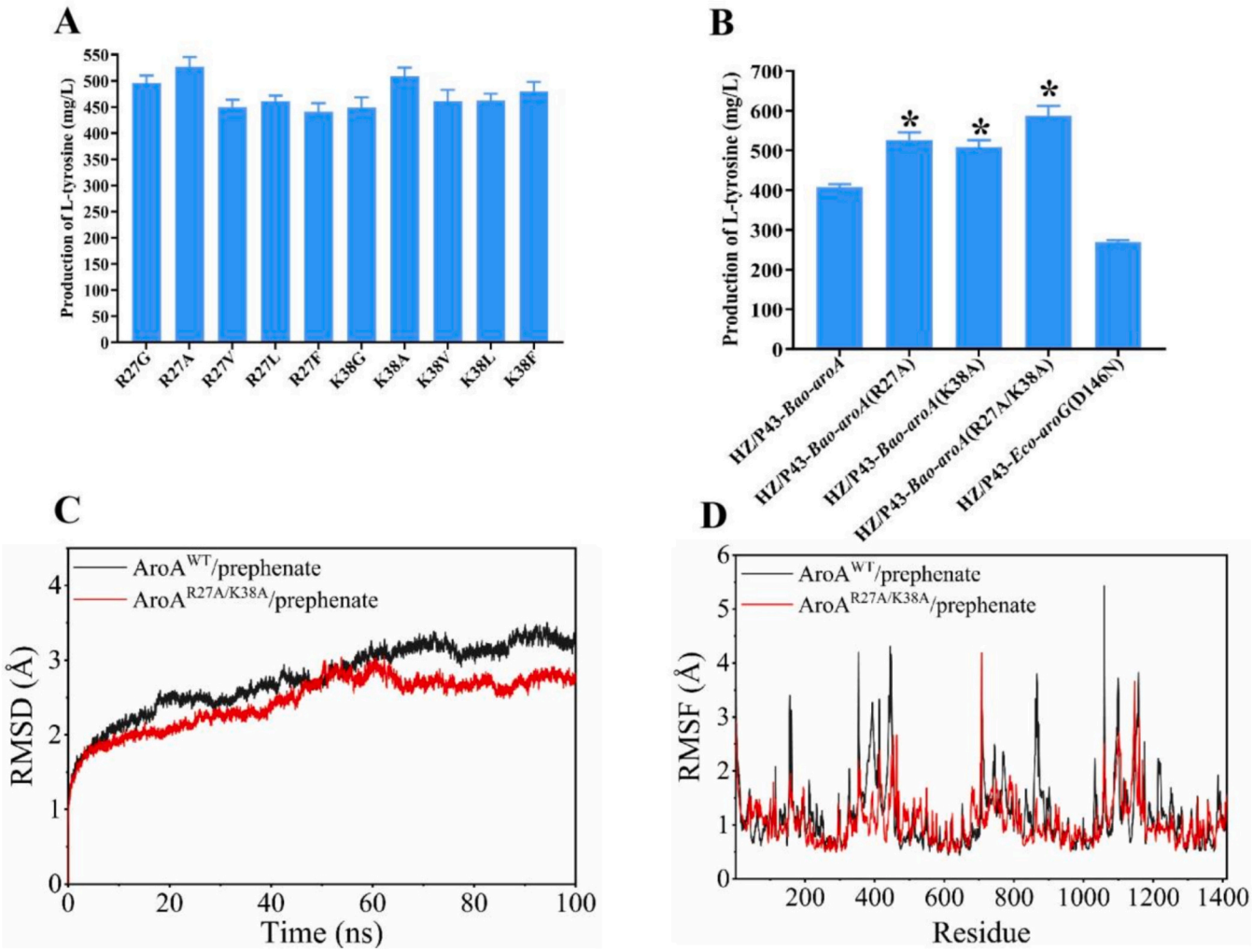

Fig. 3. Molecular dynamics simulation and the effect of AroA mutant strains on L-tyrosine synthesis. A: Different R27 and K38 mutations on L-tyrosine synthesis. B: Combination mutations on L-tyrosine synthesis. C: RMSD profiles of the AroA/prephenate complex during the 100 ns MD simulation. D: RMSF analysis of the AroA/prephenate complex under 100 ns MD simulation. (*($p < 0.05$) indicates the significant levels compared with the control.)

protein. Root mean square fluctuation (RMSF) analysis further revealed residue-specific flexibility (Fig. 3D). High RMSF values suggest a propensity for conformational changes in the protein. Conversely, low RMSF values indicate limited conformational changes, which may hinder the allosteric regulation of the protein [50]. Across the AroA tetramer, most regions showed low RMSF values, consistent with overall structural stability. Critically, mutated residues (R27A/K38A) displayed significantly lower RMSF values than wild-type counterparts under prephenate binding, suggesting that the AroA$^{R27A/K38A}$ mutant maintains enhanced stability and is less likely to achieve a conformational change.

Meanwhile, based on the trajectories from molecular dynamics simulations, we calculated the binding free energies of the complexes AroA^{WT}/prephenate and AroA$^{R27A/K38A}$/prephenate using the MM/GBSA method (Table S4). The binding free energy for AroA^{WT}/prephenate was -30.17 ± 2.66 kcal/mol, significantly stronger than that of the AroA$^{R27A/K38A}$/prephenate (-20.16 ± 1.60 kcal/mol), indicating that the R27A/K38A mutations weakened prephenate binding. This reduction likely alleviates the allosteric inhibitory effect of prephenate on AroA. Energy decomposition analysis revealed a decrease in electrostatic interactions for AroA$^{R27A/K38A}$/prephenate, which may be attributed to the loss of hydrogen bond and salt bridge. In addition, the frequency of hydrogen bond pairs such as MOL@O5 and ARG_27@HH22 was notably high at 0.5246, indicating their stability throughout the simulation period (Table S5). The average distance for most hydrogen bonds ranges from 2.7 to 2.8 Å, consistent with the typical hydrogen bond distance range. Additionally, the average angle was approximately 160°, which fallen within the standard hydrogen bond angle range of 150° to 180°. These findings suggest that residues R27 and K38 are key contributors to the hydrogen bond interactions between prephenate and AroA, characterized by both high frequency and stability. In summary, our integrated approach explained the possible mechanism behind enhanced L-tyrosine production. The designed AroA$^{R27A/K38A}$ mutant may reduce prephenate-induced allosteric inhibition to increase the catalytic efficiency. This work establishes a rational framework for optimizing metabolic enzymes in synthetic biology applications.

3.2. Rational design and molecular modification of TyrA

The biosynthesis of L-tyrosine, a precursor for various aromatic compounds, begins with the Claisen rearrangement of chorismate to prephenate [34]. Subsequently, prephenate enters the tyrosine biosynthesis pathway, where prephenate dehydrogenase (PDH) catalyzes its oxidative decarboxylation to 4-hydroxyphenylpyruvate, a rate-limiting step. Most PDHs are competitively inhibited by tyrosine and consist of a nucleotide binding domain and a dimerization domain [51]. Although certain PDHs harbor an additional ACT domain, their biochemical and structural details remain elusive [34]. According to the KEGG database, prephenate dehydrogenase (TyrA) in *B. amyloliquefaciens* HZ-12 contained an ACT domain, while prephenate served as the substrate molecule. Therefore, based on our earlier engineering of AroA, enhancing the binding affinity between TyrA protein and its substrate prephenate may improve catalytic efficiency through enzyme engineering strategies.

First, the amino acid sequence of TyrA was submitted to the SWISS-MODEL server to obtain the three-dimensional structure through homology modeling [38]. As shown in Fig. 4A, molecular docking was conducted using Autodock Vina 1.2.2 to dock prephenate with TyrA [46]. The interaction between prephenate and the TyrA model involved hydrophobic interactions by residues Val302, Asp304, and hydrogen bonds by residues Lys128, Glu330, Ile309, Val308, Gly307, Ile323, and Ser322 (Fig. 4A). To identify critical residues in the TyrA/prephenate complex, we constructed a focused alanine-scanning library targeting residues within 5 Å of the substrate. Subsequently, the mutant plasmids were electrically transformed into *B. amyloliquefaciens* HZ-12, resulting in a series of recombinant strains. L-tyrosine production was measured for all engineered strains after 36 h of cultivation in a shake flask. As shown in Fig. 4B, most mutants showed no improvement in L-tyrosine

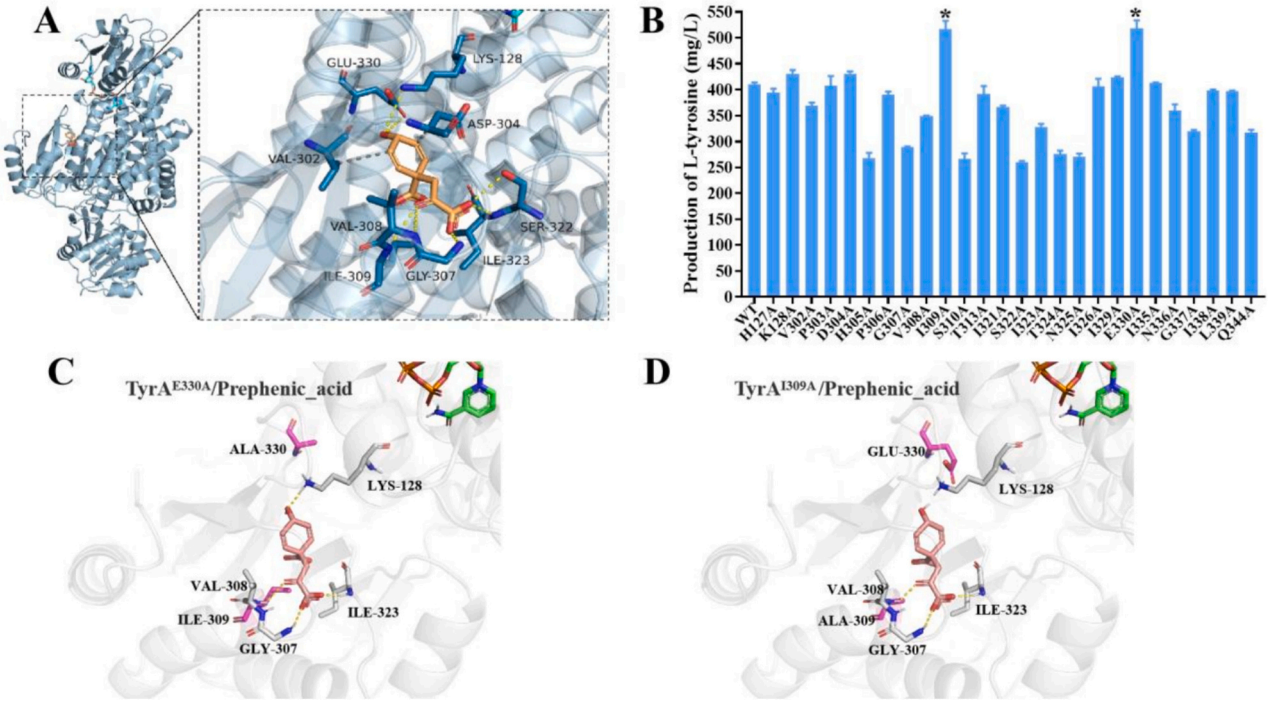

Fig. 4. Structural prediction and mutation site determination of TyrA. A: The overall structure of TyrA/prephenate complex. B: Effects of TyrA mutations on L-tyrosine production. C: The overall structure of TyrA^{E330A}/prephenate complex. D: The overall structure of TyrA^{I309A}/prephenate complex. (The right image provides a partial view. The orange stick represents the substrate small molecule, while the blue stick denotes the NAD$^+$ cofactor. The protein is depicted in blue cartoon format, with hydrogen bonding indicated by yellow dashed lines and hydrophobic interactions represented by gray dashed lines. *($p < 0.05$) indicates the significant levels compared with the control.)

production compared to the control strain (HZ/pHY-P43-*Bao-tyrA*). In contrast, the recombinant strains HZ/pHY-P43-*Bao-tyrA*^{I309A} and HZ/pHY-P43-*Bao-tyrA*^{E330A} exhibited significantly higher titers 516 mg/L and 518 mg/L, respectively, indicating that Ile309 and Glu330 may be the key residues modulating TyrA activity. These findings highlight their potential role in catalytic efficiency and justify further mechanistic studies.

In previous studies, the Ile309 and Glu330 were identified as critical residues in TyrA. To explain their mechanistic roles, we performed molecular docking of the mutant protein with its substrate and analyzed changes in interaction forces (Fig. 4A). Meanwhile, a comparison was made with the interaction forces between TyrA^{WT} and prephenate complex. As shown in Fig. 4C, the TyrA^{E330A}/prephenate complex revealed a remarkable hydrogen bonding interaction between prephenate and Lys128, resulting from the disruption of the Glu330-Lys128 salt bridge caused by the E330A mutation. This structural perturbation enhanced Lys128 flexibility, favoring hydrogen bond formation with prephenate hydroxyl groups. In contrast, the TyrA^{I309A}/prephenate complex was found to reduce hydrophobic side chains while simultaneously increasing the volume of the binding pocket (Fig. 4D). This phenomenon enhances its ability to interact with polar small molecules. Notably, our findings align with the strategy employed by Wang et al., who validated enhanced activity in the RoHpaB^{Y215A} mutant through similar mechanistic studies [48]. This work explains residue-specific functional mechanisms and provides a rational framework for engineering TyrA to optimize aromatic amino acid biosynthesis.

To evaluate the optimality of I309A and E330A for TyrA, we introduced phenylalanine, leucine, valine, and glycine substitutions at these positions, systematically reducing side chain length to probe structural effects. The results revealed that mutation of site I309 to phenylalanine, leucine, valine, or glycine did not result in a significant increase compared to I309A (Fig. 5A). In contrast, the E330G mutant achieved a titer of 546 mg/L, surpassing E330A. These results identified I309A and E330G as optimal single mutants. Subsequently, additional combinatorial mutations were performed to construct recombinant strains HZ/pHY-P43-*Bao-tyrA*$^{I309A/E330V}$. As shown in Fig. 5B, the engineering strain increased by 45 % in L-tyrosine titer (596 mg/L) compared to the control strain HZ/pHY-P43-*Bao-tyrA*. Furthermore, these mutants exhibited superior effects compared to the derived mutants in *E. coli*, indicating a synergistic effect between mutations at sites I309 and E330. Building on prior optimization [1], we further mutated the I309A and E330V sites in TyrA and obtained recombinant strains HZ/pHY-P43-UTR3-*Bao-tyrA*$^{I309A/E330V}$. As shown in Fig. 5C, the recombinant strain achieved a record titer of 647 mg/L (Fig. 5C), demonstrating the combined impact of enzyme engineering and expression optimization.

To gain further insight into the possible underlying molecular mechanisms of TyrA$^{I309A/E330V}$ mutant, we analyzed mutant dynamics through molecular simulations. As shown in Fig. 5D, RMSD analysis showed that prephenate bound to wild-type TyrA fluctuated within 2 Å, indicative of stable pocket interactions. In contrast, the TyrA$^{I309A/E330V}$ complex exhibited even tighter binding (RMSD <2 Å), suggesting enhanced structural stabilization that facilitates prephenate conversion.

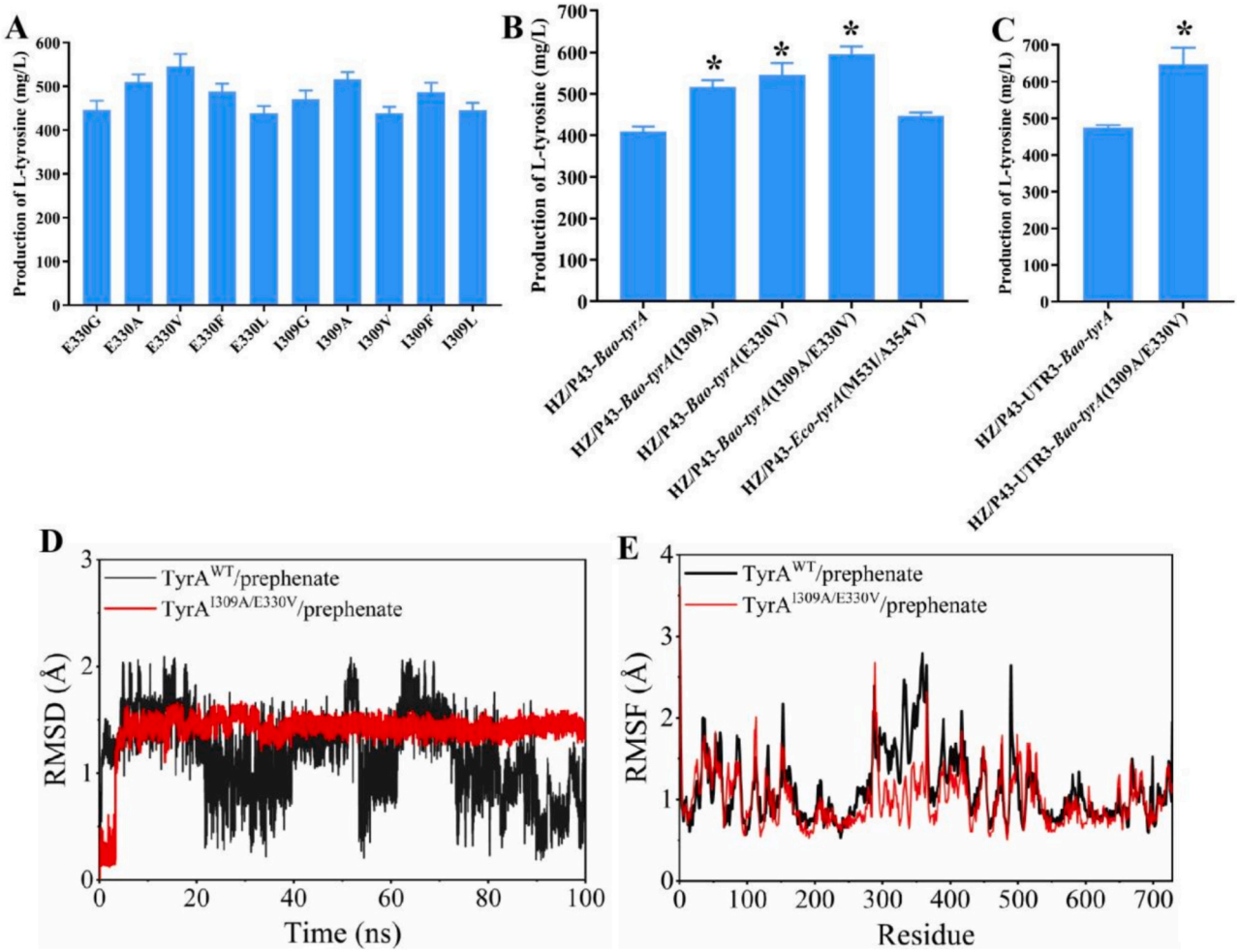

Fig. 5. Molecular dynamics simulation and the effect of TyrA mutant strains on L-tyrosine synthesis. A: Different E330 and L309 mutations on L-tyrosine synthesis. B: Combination mutations on L-tyrosine synthesis. C: Effect of combined UTR3 and mutants on L-tyrosine production. D: RMSD profiles of the TyrA/prephenate complex during the 100 ns MD simulation. E: RMSF analysis of the TyrA/prephenate complex under 100 ns MD simulation.

RMSF profiles revealed low flexibility in both complexes, with TyrA$^{I309A/E330V}$ displaying reduced residue fluctuations compared to wild-type, implying stronger substrate affinity (Fig. 5E). In addition, MM/GBSA calculations confirmed that binding free energy for the TyrA^{WT}/prephenate and TyrA$^{I309A/E330V}$/prephenate complexes were − 15.97 ± 1.95 kcal/mol and − 22.36 ± 2.72 kcal/mol, respectively. These results indicate that the TyrA$^{I309A/E330V}$ mutant exhibits a significantly stronger binding affinity for prephenate compared to the TyrA^{WT}. To date, rational engineering of prephenate dehydrogenase to enhance L-tyrosine biosynthesis remains underexplored. Here, we provide mechanistic insights into catalytic efficiency improvement through targeted protein modifications, establishing a paradigm for enzyme-driven metabolic optimization.

3.3. Co-expression of the best mutants AroA and TyrA to promote L-tyrosine accumulation

AroA and TyrA are key enzymes in the L-tyrosine biosynthetic pathway. Previous studies have demonstrated that overexpression of aroA or tyrA genes significantly increases the yield of L-tyrosine [27]. However, due to the complex nature of metabolic networks, the enhancing effect on L-tyrosine synthesis is attenuated. Wang et al. increased gleenol production in *E. coli* through coordinated expression of sinense sesquiterpene synthase and IDI [52]. It is evident that the utilization of co-expression strategies for key genes has emerged as an effective approach.

Therefore, to further improve the ability of L-tyrosine synthesis, we performed co-expression of the *aroA*$^{R27A/K38A}$ and *tyrA*$^{I309A/E330V}$ genes, and the original genes *aroA* and *tyrA* was served as controls. The recombinant strains HZ/pHY-P43-UTR3-*Bao-tyrA*-RBS-*aroA* and HZ/pHY-P43-UTR3-*Bao-tyrA*$^{I309A/E330V}$-RBS-*aroA*$^{R27A/K38A}$ were obtained by electro-transformation. As shown in Fig. 6, the co-expression of the mutant *aroA*$^{R27A/K38A}$ and *tyrA*$^{I309A/E330V}$ resulted in a significant enhancement in L-tyrosine production, reaching up to 970 mg/L. This is notably higher than the yields obtained from the individual expression of *aroA*$^{R27A/K38A}$ (587 mg/L) and *tyrA*$^{I309A/E330V}$ (647 mg/L), as well as the co-expression of the wild-type *tyrA* and *aroA* genes (746 mg/L). These results highlight the efficacy of co-expressing optimized pathway genes in enhancing L-tyrosine production.

3.4. Modification of the branching pathways of matter and energy

Previous studies have demonstrated that protein engineering can improve the catalytic efficiency of AroA and TyrA. However, the biosynthesis of L-tyrosine involves a complex metabolic pathway with multiple genes and different regulatory mechanisms (Fig. 7A). Molecular modification of key enzymes in this pathway represents only one aspect of the intervention. It is equally crucial to optimize the competitive metabolic pathways to augment the flux through the L-tyrosine synthesis pathway and improve carbon flux efficiency. Furthermore, rational engineering of microbial metabolism represents a viable approach to enhance microbial metabolic efficiency and optimize target product synthesis. For instance, Zamboni et al. have successfully obtained an engineering strain of *Bacillus subtilis* by knocking out the cytochrome *bd* oxidase gene, resulting in a 40 % reduction in cell maintenance requirements and a 30 % increase in bacterial riboflavin production compared to the wild-type strain [53]. To further improve the ability of host strain synthesis, we introduced the co-expression plasmids into *B. amyloliquefaciens* HZ-12 derivatives.

As shown in Fig. 7B, the deletion of the tryptophan pathway led to a significant 33 % increase in L-tyrosine production, achieving 1262 mg/L compared to the HZ/S6–36 strain. In contrast, deletions in other competing pathways did not significantly affect L-tyrosine production. These findings suggest that the tryptophan pathway plays a crucial role in carbon flux competition. By eliminating this pathway, carbon flux is effectively redirected, resulting in substantial accumulation of L-tyrosine. Furthermore, the deletion of the *ythAB* gene markedly enhanced L-tyrosine accumulation, achieving 1414 mg/L, which represents a 49 % increase relative to the HZ/S6-36 strain (Fig. 7C). Subsequent stacking knockout of *trpE* and *ythAB* further contribute to an additional improvement in yield. The engineered strains HZ5A/S6-36, HZ5AΔ*trpE*/S6-36, and HZ5AΔ*trpE*Δ*ythAB*/S6-36 were obtained and their fermentation results are shown in Fig. 7D. Their L-tyrosine yields reached 1.25 g/L, 1.40 g/L, and 1.76 g/L, respectively. Notably, the engineered strain HZ5AΔ*trpE*Δ*ythAB*/S6-36 showed a 69% increase in L-tyrosine production compared to the starting strain HZ/S6-36. These studies suggest that modifying competing metabolic pathways and energy metabolism pathways is an effective strategy to enhance L-tyrosine production.

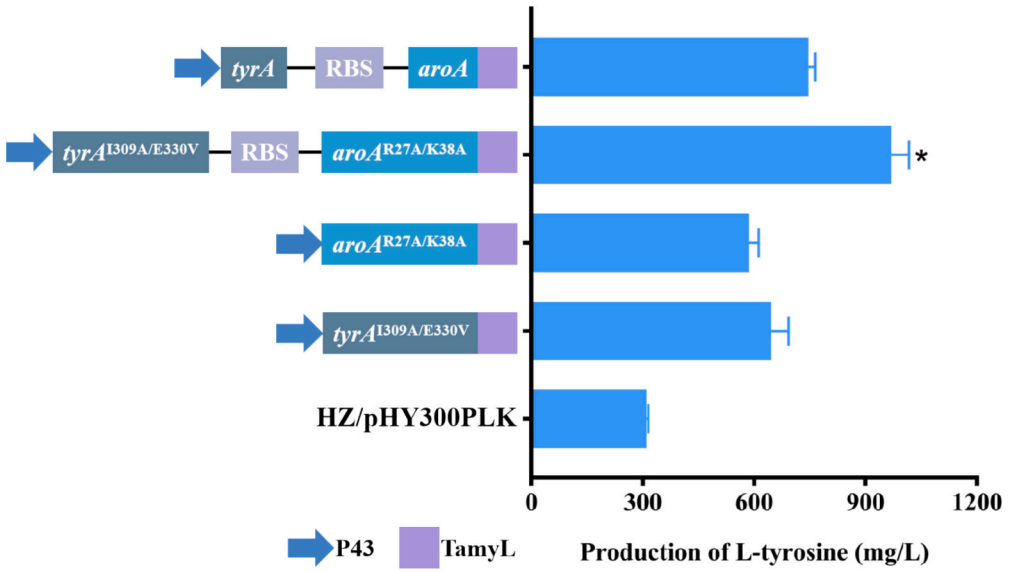

Fig. 6. Effect of the tandem and fusion expression between *aroA*$^{R27A/K38A}$ and *tyrA*$^{I309A/E330V}$ on L-tyrosine synthesis. (*($p < 0.05$) indicates the significant levels compared with the control.)

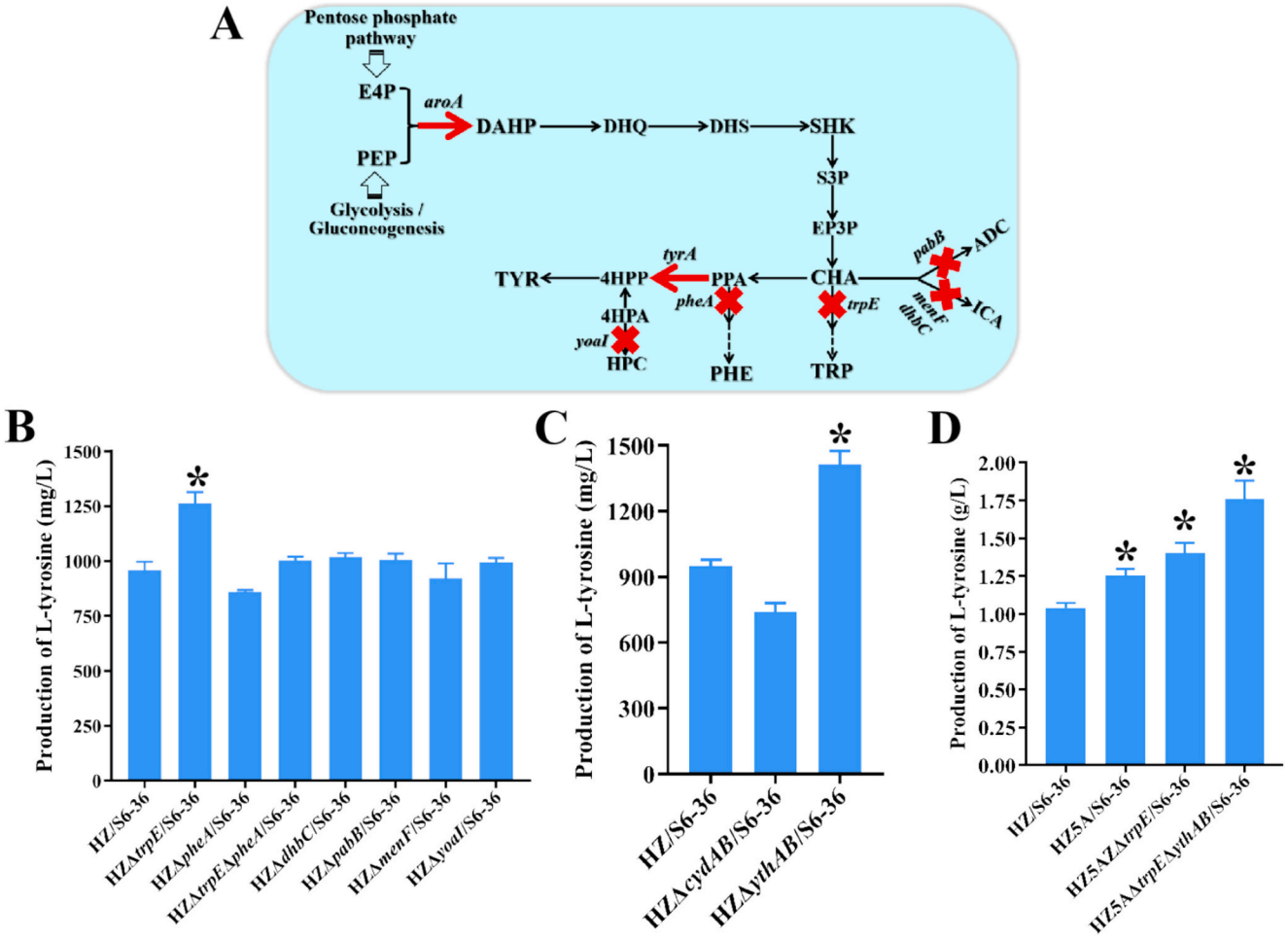

Fig. 7. Effects of different host strains on L-tyrosine synthesis. A: E4P, erythrose 4-phosphate; PEP, phosphoenolpyruvate; DAHP, 3-deoxyd-arabino-heptulosonic acid 7-phosphate; DHQ, 3-dehydroquinic acid; DHS, 3-dehydroshikimate; SHK, shikimate; S3P, shikimate 3-phosphate; EPSP, 5-enolpyruvylshikimate-3-phosphate; CHA, chorismate; PPA, prephenate; HPP, 4-hydroxyphenylpyruvate; Tyr, l-tyrosine. B: The effect of competitive pathway gene deletion on L-tyrosine synthesis. C: The effect of energy metabolism gene deletion on L-tyrosine synthesis. D: The effect of host strain replacement and stacking knockout *trpE* and *ythAB* on L-tyrosine synthesis. (*($p < 0.05$) indicates the significant levels compared with the control.)

3.5. Optimization of fermentation process for recombinant bacterial strains

Due to the requirement for appropriate culture media and conditions for microbial growth, optimizing traditional fermentation processes and fermentation medium is also crucial for increasing L-tyrosine production through microbial fermentation. The temperature, pH value, and composition of the culture medium during fermentation significantly influence the physiological state of the fermenting strains and enzyme activity and thus influence the accumulation of metabolic product [54]. To address these factors, we plans to further improve the production of L-tyrosine by optimizing the composition of the culture medium.

To identify the renewable carbon resources, the initial carbon source was investigated. Xylose emerged as the optimal choice, maximizing titer (Fig. 8A), due to its efficient assimilation via xylose isomerase (XI) and xylulose kinase, which funnel xylulose-5-phosphate into the pentose phosphate pathway (PPP). PPP metabolites (glucose-6-phosphate and glyceraldehyde-3-phosphate) feed glycolysis, providing energy and precursors for aromatic biosynthesis. We attribute this preference to enhanced xylose catabolism, which boosts flux through PPP, elevating pools of the key precursors erythrose-4-phosphate (E4P) and phosphoenolpyruvate (PEP) for L-tyrosine synthesis. Subsequently, optimization of the xylose concentration revealed that the highest L-tyrosine yield was achieved at a concentration of 44 g/L (Fig. 8B). For nitrogen sources, the results demonstrated that the highest yield of L-tyrosine was achieved at an ammonium sulfate concentration of 10 g/L (Fig. 8C). Previous experiments indicated that sodium nitrate enhanced dissolved oxygen levels [55]. Therefore, various concentrations of sodium nitrate were further added and it was observed that the maximum L-tyrosine yield occurred at a concentration of 10 g/L (Fig. 8D). Subsequently, the yeast powder and peptone concentrations were optimized resulting in a final increase in L-tyrosine yield to 9.39 g/L (Fig. 8E and F). Collectively, medium optimization significantly enhanced L-tyrosine production, demonstrating the importance of substrate selection and nutrient balancing in microbial metabolic engineering.

4. Conclusions

This study carried out a structurally directed rational design of the key enzymes DAHP synthase (AroA) and prephenate dehydrogenase (TyrA) in the metabolic pathway. Beneficial mutants were identified that significantly promote product synthesis. Then, this study further combined metabolic engineering strategies and fermentation process optimization to achieve a large accumulation of L-tyrosine. The yield of L-tyrosine reached 9.39 g/L when used xylose as a carbon source. This study was the first report of computer-aided rational design targeting both AroA and TyrA, yielding beneficial mutants that provided valuable genetic resources for future metabolic engineering. In addition, it is also

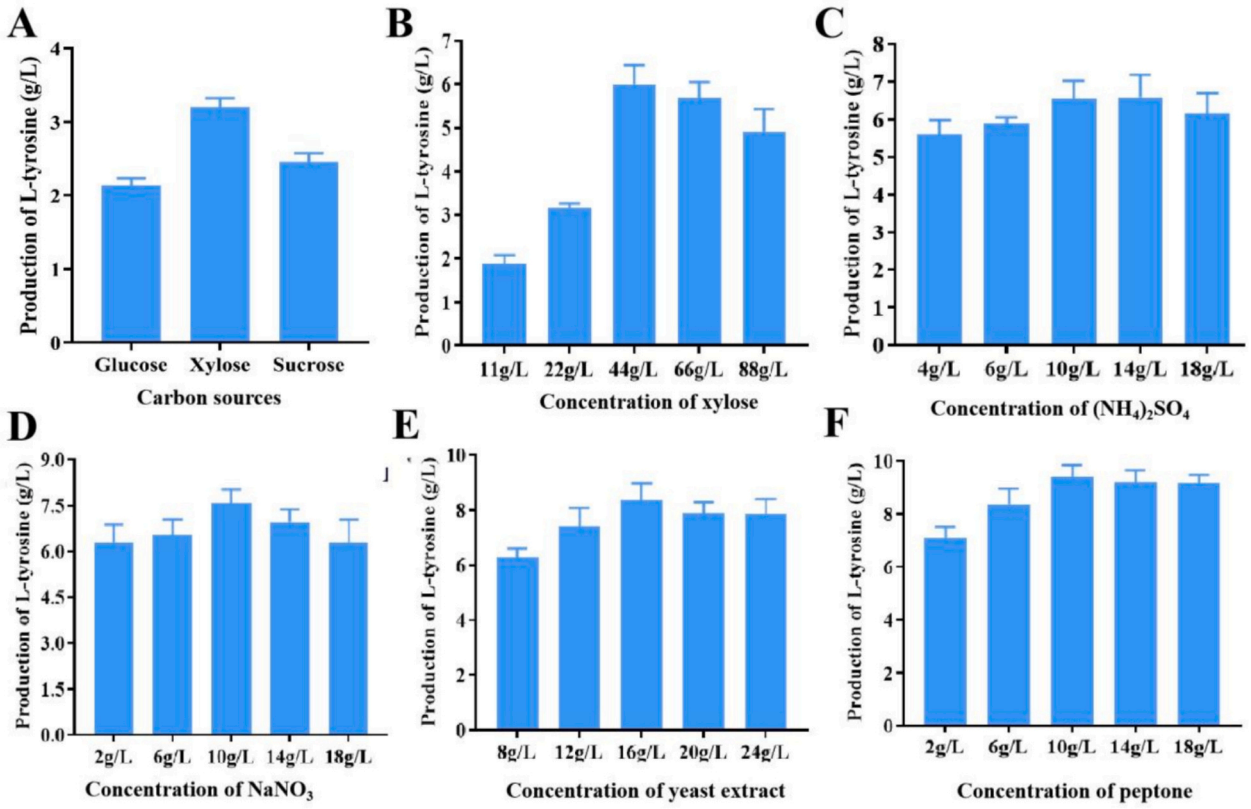

Fig. 8. Effect of fermentation medium optimization on L-tyrosine synthesis. A: The influence of different types of carbon sources on L-tyrosine synthesis. B: The effect of different concentrations of xylose on L-tyrosine synthesis. C: The effect of different concentrations of ammonium sulfate on L-tyrosine synthesis. D: The effect of different concentrations of sodium nitrate on L-tyrosine synthesis. E: The effect of different concentrations of yeast extract powder on L-tyrosine synthesis. F: The effect of different concentrations of peptone on L-tyrosine synthesis.

an environmentally friendly and sustainable method of synthesis to use xylose as a substrate.

CRediT authorship contribution statement

Anying Ji: Writing – original draft, Visualization, Validation, Investigation, Formal analysis, Data curation, Conceptualization. **Dian Zou:** Writing – original draft, Methodology, Investigation, Funding acquisition, Formal analysis, Data curation. **Aimin Ma:** Writing – review & editing, Supervision, Resources, Project administration. **Xuetuan Wei:** Writing – review & editing, Supervision, Resources, Project administration, Methodology, Funding acquisition, Conceptualization.

Declaration of competing interest

The authors declare no conflicts of interest.

Acknowledgement

This study was supported by the National Natural Science Foundation of China (Nos. 32171423, 32371493), the Key Research and Development Program of Hubei Province (No. 2022BBA0040), the National Key Research and Development Program of China (No. 2022YFF1000700), and China Postdoctoral Science Foundation (No. 2024M751037).

Appendix A. Supplementary data

Supplementary data to this article can be found online at https://doi.org/10.1016/j.ijbiomac.2025.142076.

References

[1] A. Ji, P. Bao, A. Ma, X. Wei, An efficient Prephenate dehydrogenase gene for the biosynthesis of L-tyrosine: Gene Mining, sequence analysis, and expression optimization, Foods 12 (16) (2023).
[2] E. Kurpejović, A. Burgardt, G.M. Bastem, N. Junker, V.F. Wendisch, B. Sariyar Akbulut, Metabolic engineering of Corynebacterium glutamicum for l-tyrosine production from glucose and xylose, J. Biotechnol. 363 (2023) 8–16.
[3] J. Ping, L. Wang, Z. Qin, Z. Zhou, J. Zhou, Synergetic engineering of *Escherichia coli* for efficient production of l-tyrosine, Synth Syst Biotechnol 8 (4) (2023) 724–731.
[4] S.C. Kim, B.E. Min, H.G. Hwang, S.W. Seo, G.Y. Jung, Pathway optimization by re-design of untranslated regions for L-tyrosine production in *Escherichia coli*, Sci. Rep. 5 (2015) 13853.
[5] C.A. Schenck, H.A. Maeda, Tyrosine biosynthesis, metabolism, and catabolism in plants, Phytochemistry 149 (2018) 82–102.
[6] J. Wang, X. Shen, J. Rey, Q. Yuan, Y. Yan, Recent advances in microbial production of aromatic natural products and their derivatives, Appl. Microbiol. Biotechnol. 102 (1) (2018) 47–61.
[7] J. Bongaerts, M. Krämer, U. Müller, L. Raeven, M. Wubbolts, Metabolic engineering for microbial production of aromatic amino acids and derived compounds, Metab. Eng. 3 (4) (2001) 289–300.
[8] G. Gosset, Production of aromatic compounds in bacteria, Curr. Opin. Biotechnol. 20 (6) (2009) 651–658.
[9] Y. Lin, Y. Yan, Biosynthesis of caffeic acid in *Escherichia coli* using its endogenous hydroxylase complex, Microb. Cell Fact. 11 (2012) 42.
[10] F.S. Sariaslani, Development of a combined biological and chemical process for production of industrial aromatics from renewable resources, Annu. Rev. Microbiol. 61 (2007) 51–69.
[11] S.F. Yuan, H.S. Alper, Metabolic engineering of microbial cell factories for production of nutraceuticals, Microb. Cell Fact. 18 (1) (2019) 46.
[12] Z.W. Luo, S.Y. Lee, Biotransformation of p-xylene into terephthalic acid by engineered *Escherichia coli*, Nat. Commun. 8 (2017) 15689.
[13] S.Y. Park, D. Yang, S.H. Ha, S.Y. Lee, Metabolic engineering of microorganisms for the production of natural compounds, Advanced Biosystems 2 (1) (2018).
[14] L. Liu, Z. Zhao, R. Zhu, X. Qin, Can national environmental protection supervision and control have a lasting impact on corporate production efficiency? - an empirical study based on the multi-phase difference-in-difference model, Environ. Sci. Pollut. Res. Int. 29 (37) (2022) 56136–56153.
[15] F. Wu, P. Cao, G. Song, W. Chen, Q. Wang, Expanding the repertoire of aromatic chemicals by microbial production, J. Chem. Technol. Biotechnol. 93 (10) (2018).

[16] S. Noda, A. Kondo, Recent advances in microbial production of aromatic chemicals and derivatives, Trends Biotechnol. 35 (8) (2017) 785–796.
[17] B. Thompson, M. Machas, D.R. Nielsen, Creating pathways towards aromatic building blocks and fine chemicals, Curr. Opin. Biotechnol. 36 (2015) 1–7.
[18] Y. Gu, X. Xu, Y. Wu, T. Niu, Y. Liu, J. Li, G. Du, L. Liu, Advances and prospects of *Bacillus subtilis* cellular factories: from rational design to industrial applications, Metab. Eng. 50 (2018) 109–121.
[19] L. Liu, J. Li, Y. Gai, Z. Tian, Y. Wang, T. Wang, P. Liu, Q. Yuan, H. Ma, S.Y. Lee, D. Zhang, Protein engineering and iterative multimodule optimization for vitamin B(6) production in *Escherichia coli*, Nat. Commun. 14 (1) (2023) 5304.
[20] M. Pagliaro, An industry in transition: the chemical industry and the megatrends driving its forthcoming transformation, Angew. Chem. Int. Ed. Engl. 58 (33) (2019) 11154–11159.
[21] B. Zeng, Y. Lai, L. Liu, J. Cheng, Y. Zhang, J. Yuan, Engineering *Escherichia coli* for high-yielding Hydroxytyrosol synthesis from biobased l-tyrosine, J. Agric. Food Chem. 68 (29) (2020) 7691–7696.
[22] S. Panda, J.F.J. Zhou, M. Feigis, E. Harrison, X. Ma, V. Fung Kin Yuen, R. Mahadevan, K. Zhou, Engineering *Escherichia coli* to produce aromatic chemicals from ethylene glycol, Metab. Eng. 79 (2023) 38–48.
[23] X. Ouyang, Y. Liu, R. Qu, M. Tian, T. Yang, R. Zhu, H. Gao, M. Jin, J. Huang, Optimizing protein-Glutaminase expression in *Bacillus subtilis*, Curr. Microbiol. 78 (5) (2021) 1752–1762.
[24] L. Liu, Y. Liu, H.D. Shin, R.R. Chen, N.S. Wang, J. Li, G. Du, J. Chen, Developing *Bacillus* spp. as a cell factory for production of microbial enzymes and industrially important biochemicals in the context of systems and synthetic biology, Appl. Microbiol. Biotechnol. 97 (14) (2013) 6113–6127.
[25] Z. Luo, Y. Yan, S. Du, Y. Zhu, F. Pan, R. Wang, Z. Xu, X. Xu, S. Li, H. Xu, Recent advances and prospects of *Bacillus amyloliquefaciens* as microbial cell factories: from rational design to industrial applications, Crit. Rev. Biotechnol. 43 (7) (2023) 1073–1091.
[26] P. Gollnick, P. Babitzke, E. Merino, C. Yanofsky, Aromatic Amino Acid Metabolism in *Bacillus subtilis*, John Wiley & Sons, Ltd, 2014.
[27] Y. Xu, Y. Li, Z. Wu, Y. Lu, G. Tao, L. Zhang, Z. Ding, G. Shi, Combining precursor-directed engineering with modular designing: an effective strategy for De novo biosynthesis of l-DOPA in *Bacillus licheniformis*, ACS Synth. Biol. 11 (2) (2022) 700–712.
[28] Y. Xu, Y. Li, L. Zhang, Z. Ding, Z. Gu, G. Shi, Unraveling the specific regulation of the shikimate pathway for tyrosine accumulation in *Bacillus licheniformis*, J. Ind. Microbiol. Biotechnol. 46 (8) (2019) 1047–1059.
[29] Y. Zhan, J. Shi, Y. Xiao, F. Zhou, H. Wang, H. Xu, Z. Li, S. Yang, D. Cai, S. Chen, Multilevel metabolic engineering of *Bacillus licheniformis* for de novo biosynthesis of 2-phenylethanol, Metab. Eng. 70 (2022) 43–54.
[30] B. Kim, R. Binkley, H.U. Kim, S.Y. Lee, Metabolic engineering of *Escherichia coli* for the enhanced production of l-tyrosine, Biotechnol. Bioeng. 115 (10) (2018) 2554–2564.
[31] Y.M. Ger, S.L. Chen, H.J. Chiang, D. Shiuan, A single Ser-180 mutation desensitizes feedback inhibition of the phenylalanine-sensitive 3-deoxy-D-arabino-heptulosonate 7-phosphate (DAHP) synthetase in *Escherichia coli*, J. Biochem. 116 (5) (1994) 986–990.
[32] S. Wang, D. Liu, M. Bilal, W. Wang, X. Zhang, Uncovering the role of PhzC as DAHP synthase in shikimate pathway of Pseudomonas chlororaphis HT66, Biology (Basel) 11 (1) (2022).
[33] D. Cui, A. Deng, H. Bai, Z. Yang, Y. Liang, Z. Liu, Q. Qiu, L. Wang, S. Liu, Y. Zhang, Y. Shi, J. Qi, T. Wen, Molecular basis for feedback inhibition of tyrosine-regulated 3-deoxy-d-arabino-heptulosonate-7-phosphate synthase from *Escherichia coli*, J. Struct. Biol. 206 (3) (2019) 322–334.
[34] I.G. Shabalin, A. Gritsunov, J. Hou, J. Sławek, C.D. Miks, D.R. Cooper, W. Minor, D. Christendat, Structural and biochemical analysis of *Bacillus anthracis* prephenate dehydrogenase reveals an unusual mode of inhibition by tyrosine via the ACT domain, FEBS J. 287 (11) (2020) 2235–2255.
[35] C. Zhou, T. Chen, A. Gu, Z. Hu, Y. Li, T. Gong, J. Chen, J. Yang, P. Zhu, Combining protein and metabolic engineering to achieve green biosynthesis of 12β-O-Glc-PPD in *Saccharomyces cerevisiae*, Green Chem. 25 (4) (2023) 1356–1367.
[36] Y.-O. Bao, M. Zhang, H. Li, Z. Wang, J. Zhou, Y. Yi, F. Li, L. Ye, H. Li, H. Jin, C. He, M. Ye, Functional characterization and protein engineering of a glycosyltransferase GcCGT to produce flavone 6,8-Di-C- and 6-C-4′-O-glycosides, ACS Catal. 14 (2) (2024) 1075–1082.
[37] C. Jiang, D. Zou, X. Jiang, W. Han, K. Chen, A. Ma, X. Wei, Enhancement of Green production of Heme by deleting odor-related genes from *Bacillus amyloliquefaciens* based on CRISPR/Cas9n, J. Agric. Food Chem. 72 (29) (2024) 16412–16422.
[38] A. Waterhouse, M. Bertoni, S. Bienert, G. Studer, G. Tauriello, R. Gumienny, F. T. Heer, T.A.P. de Beer, C. Rempfer, L. Bordoli, R. Lepore, T. Schwede, SWISS-MODEL: homology modelling of protein structures and complexes, Nucleic Acids Res. 46 (W1) (2018) W296–w303.
[39] A.R. Nazmi, E.J.M. Lang, Y. Bai, T.M. Allison, M.H. Othman, S. Panjikar, V. L. Arcus, E.J. Parker, Interdomain conformational changes provide allosteric regulation en route to Chorismate, J. Biol. Chem. 291 (42) (2016) 21836–21847.
[40] S.H. Light, W.F. Anderson, The diversity of allosteric controls at the gateway to aromatic amino acid biosynthesis, Protein Sci. 22 (4) (2013) 395–404.
[41] C.A. Schenck, C.K. Holland, M.R. Schneider, Y. Men, S.G. Lee, J.M. Jez, H. A. Maeda, Molecular basis of the evolution of alternative tyrosine biosynthetic routes in plants, Nat. Chem. Biol. 13 (9) (2017) 1029–1035.
[42] S. Pratap, A. Dev, V. Kumar, R. Yadav, M. Narwal, S. Tomar, P. Kumar, Structure of Chorismate mutase-like domain of DAHPS from *Bacillus subtilis* complexed with novel inhibitor reveals conformational plasticity of active site, Sci. Rep. 7 (1) (2017) 6364.
[43] I.A. Shumilin, R. Bauerle, J. Wu, R.W. Woodard, R.H. Kretsinger, Crystal structure of the reaction complex of 3-deoxy-D-arabino-heptulosonate-7-phosphate synthase from *Thermotoga maritima* refines the catalytic mechanism and indicates a new mechanism of allosteric regulation, J. Mol. Biol. 341 (2) (2004) 455–466.
[44] H. Liu, W. Wei, Z. Pang, S. Gu, W. Song, C. Gao, X. Chen, J. Liu, L. Guo, J. Wu, L. Liu, Protein engineering, cofactor engineering, and surface display engineering to achieve whole-cell catalytic production of chondroitin sulfate a, Biotechnol. Bioeng. 120 (7) (2023) 1784–1796.
[45] H.F. Son, H. Yu, J. Hong, D. Lee, I.K. Kim, K.J. Kim, Structure-guided protein engineering of Glyceraldehyde-3-phosphate dehydrogenase from *Corynebacterium glutamicum* for dual NAD/NADP cofactor specificity, J. Agric. Food Chem. 71 (46) (2023) 17852–17859.
[46] J. Eberhardt, D. Santos-Martins, A.F. Tillack, S. Forli, AutoDock Vina 1.2.0: new docking methods, expanded force field, and Python bindings, J. Chem. Inf. Model. 61 (8) (2021) 3891–3898.
[47] D. Mhaindarkar, R. Gasper, N. Lupilov, E. Hofmann, L.I. Leichert, Loss of a conserved salt bridge in bacterial glycosyl hydrolase BgIM-G1 improves substrate binding in temperate environments, Commun Biol 1 (2018) 171.
[48] H. Wang, S. Wang, J. Wang, X. Shen, X. Feng, S. Yuan, X. Sun, Q. Yuan, Engineering a prokaryotic non-P450 hydroxylase for 3'-hydroxylation of flavonoids, ACS Synth Biol 11 (11) (2022) 3865–3873.
[49] Y. Maruyama, R. Igarashi, Y. Ushiku, A. Mitsutake, Analysis of protein folding simulation with moving root mean square deviation, J. Chem. Inf. Model. 63 (5) (2023) 1529–1541.
[50] W. Xia, Y. Gao, X. Fang, L. Jin, R. Liu, L.S. Wang, Y. Deng, J. Gao, H. Yang, W. Wu, H. Gao, Simulated gastrointestinal digestion of walnut protein yields anti-inflammatory peptides, Food Chem. 445 (2024) 138646.
[51] J. Song, C.A. Bonner, M. Wolinsky, R.A. Jensen, The TyrA family of aromatic-pathway dehydrogenases in phylogenetic context, BMC Biol. 3 (2005) 13.
[52] Q. Wang, P. Qi, C. Zhao, Y. Zhang, L. Wang, H. Yu, Tandem expression of Ganoderma sinense sesquiterpene synthase and IDI promotes the production of gleenol in *E. Coli*, Appl. Microbiol. Biotechnol. 106 (23) (2022) 7779–7791.
[53] N. Zamboni, N. Mouncey, H.P. Hohmann, U. Sauer, Reducing maintenance metabolism by metabolic engineering of respiration improves riboflavin production by *Bacillus subtilis*, Metab. Eng. 5 (1) (2003) 49–55.
[54] D. Li, X. Wang, Z. Qin, S. Yu, J. Chen, J. Zhou, Combined engineering of l-sorbose dehydrogenase and fermentation optimization to increase 2-keto-l-gulonic acid production in *Escherichia coli*, Bioresour. Technol. 372 (2023) 128672.
[55] R. Patnaik, R.R. Zolandz, D.A. Green, D.F. Kraynie, L-tyrosine production by recombinant *Escherichia coli*: fermentation optimization and recovery, Biotechnol. Bioeng. 99 (4) (2008) 741–752.